

Label-Efficient LiDAR Semantic Segmentation with 2D-3D Vision Transformer Adapters

Julia Hindel*, Rohit Mohan*, Jelena Bratulić, Daniele Cattaneo, Thomas Brox, and Abhinav Valada

Abstract—LiDAR semantic segmentation models are typically trained from random initialization as universal pre-training is hindered by the lack of large, diverse datasets. Moreover, most point cloud segmentation architectures incorporate custom network layers, limiting the transferability of advances from vision-based architectures. Inspired by recent advances in universal foundation models, we propose BALViT, a novel approach that leverages frozen vision models as amodal feature encoders for learning strong LiDAR encoders. Specifically, BALViT incorporates both range-view and bird’s-eye-view LiDAR encoding mechanisms, which we combine through a novel 2D-3D adapter. While the range-view features are processed through a frozen image backbone, our bird’s-eye-view branch enhances them through multiple cross-attention interactions. Thereby, we continuously improve the vision network with domain-dependent knowledge, resulting in a strong label-efficient LiDAR encoding mechanism. Extensive evaluations of BALViT on the SemanticKITTI and nuScenes benchmarks demonstrate that it outperforms state-of-the-art methods on small data regimes. We make the code and models publicly available at <http://balvit.cs.uni-freiburg.de>.

I. INTRODUCTION

Self-driving vehicles often rely on LiDAR sensors to semantically perceive their surroundings due to their invariance to lighting conditions [1], [2]. However, LiDAR semantic segmentation methods typically follow a fully supervised learning paradigm [3], [4], which requires labor-intensive data collection and manual labeling of large-scale point cloud datasets. Recently, self-supervised methods have been introduced, enabling the pre-training of neural networks without the need for ground truth labels. Pre-training improves the performance of the network when fine-tuned on a small labeled dataset [3]–[5]. While these techniques excel with images [6]–[8] and natural language, the performance improvements are limited for LiDAR data. This is primarily due to the absence of large and diverse pre-training datasets that cover the significant domain shifts between different LiDAR sensors [9], [10]. Consequently, label-efficient techniques that leverage models pre-trained on other modalities are required. Prior work in this direction focuses on extending vision and language foundation models [11], [12] for 3D perception by adding a separate network branch [13]–[17] or directly distilling network features [3], [18], as shown in Fig. 1. However, these methods still train a randomly initialized LiDAR sub-network and require time-synchronized camera and LiDAR streams with accurate extrinsic calibration.

* Authors contributed equally to this work.
Department of Computer Science, University of Freiburg, Germany.
This work was funded by the Deutsche Forschungsgemeinschaft (DFG, German Research Foundation) – SFB 1597 – 499552394.

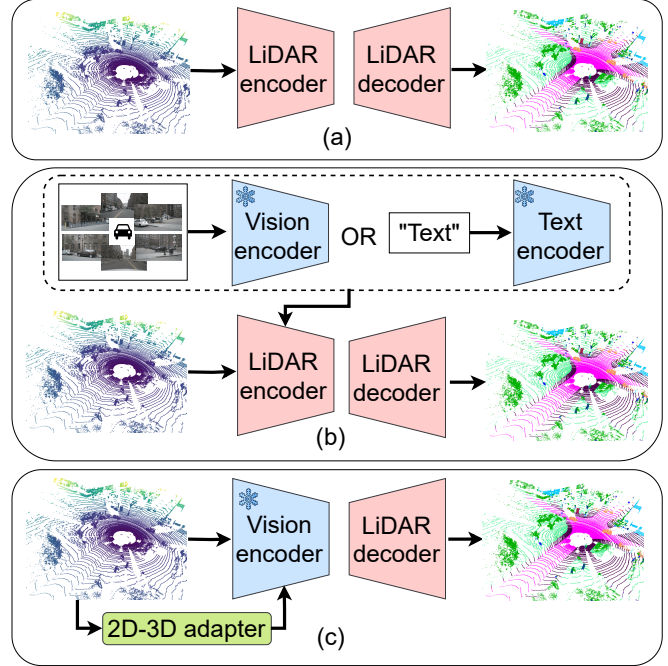


Fig. 1. Different learning paradigms for LiDAR semantic segmentation. Learned modules are colored in red and frozen components in blue. (a) Traditional methods leverage randomly initialized LiDAR networks. (b) Vision or language foundation models are employed to distill knowledge into tailored LiDAR architectures. (c) Transferring a pre-trained vision model into the LiDAR domain using a range-view projection and a 2D-3D adapter (ours).

Another line of work follows the paradigm of a universal foundation model where only the patch embedding and the decoder are tailored to 3D point clouds [19]–[21]. Consequently, these methods can benefit from strong pre-trained feature extractors and can easily leverage advances in the field of foundation models [19]. However, RangeViT [19] shows the need for full fine-tuning of vision models for outdoor LiDAR segmentation, which is computationally expensive and infeasible when only a small number of labeled scans are available. Further, we demonstrate that adapters and visual prompt tuning methods initially introduced for 2D computer vision tasks do not readily generalize to label-efficient outdoor 3D point cloud segmentation. Consequently, we highlight the need for domain-aware adapters that incorporate the geometric constraints of 3D sparse point clouds to transform a pre-trained vision model into a robust 3D segmenter.

In this paper, we introduce BALViT (Bird-Eye-View Adapted LiDAR ViT), which seamlessly incorporates vision models with a novel 2D-3D adapter for label-efficient LiDAR semantic segmentation. In particular, we extend the vision

model-based network RangeViT [19] with a lightweight, polar Bird’s-Eye View (BEV)-based adapter. We reason that vision models excel at detecting object shapes, whereas our adapter incorporates geometric reasoning. Finally, we introduce a separate BEV decoder branch to address and correct misclassifications, ensuring the model generates accurate 3D semantic segmentation by refining the output through complementary branches.

Our main contributions can be summarized as follows:

- BALViT, a novel LiDAR semantic segmentation architecture that leverages pre-trained vision models as a backbone.
- A newly-designed 2D-3D adapter for label-efficient refinement of vision models for sparse 3D segmentation.
- Extensive evaluations and ablation study on two datasets and tasks with a focus on minimal labeled data.
- Publicly available code and pre-trained models at <http://balvit.cs.uni-freiburg.de>.

II. RELATED WORK

LiDAR Semantic Scene Segmentation: Point cloud semantic segmentation networks are commonly categorized according to the chosen representation. Voxel-based architectures subsample points according to coordinate grids before applying 3D convolutions [22] or radial attention [23]. On the other hand, point-based methods extract features directly from points using multi-layer perceptrons [24] or transformer-based architectures [25], [26]. However, both voxel-based and point-based approaches are computationally expensive and leverage custom architectures that do not benefit from advances in 2D computer vision research. The third category of LiDAR segmentation models convert point clouds into 2D projections, enabling the integration of standard computer vision architectures [19], [27], [28]. PolarNet proposes to map point cloud features into a BEV projection before applying circular padded convolutions [27]. RangeViT [19], FRNet [28], and RangeFormer [29] convert the point cloud into multichannel range projections. Further, RangeViT [19] motivates the development of LiDAR architectures that closely resemble 2D vision architectures and pairs LiDAR-specific patch embeddings and decoder layers with a standard ViT backbone for semantic segmentation. However, RangeViT requires end-to-end fine-tuning on 3D data and suffers from the perspective distortion of range-views. Consequently, we propose to extend RangeViT with a parameter-efficient 2D-3D adapter to enhance the geometric prediction capabilities, effectively improving performance in small data settings.

LiDAR Representation Learning: Self-supervised representation learning focuses on pre-training a LiDAR segmentation model with unlabeled data. While SegContrast [5] and TARL [4] perform contrastive learning between class-agnostic segments, BEVContrast [30] applies its contrastive loss between BEV projections of two augmented point clouds. Masked autoencoders, on the other hand, are trained for surface reconstruction [31] or occupancy map prediction [32]. Another family of approaches leverages geometric and time-aligned camera-LiDAR sensor input in addition to vision

foundation models to pre-train 3D segmentation models. Commonly, the vision model extracts class-agnostic segments and supervises the 3D branch with their respective cross-modal alignment in feature space [3], [18], [33], [34]. Another direction of research extends the vision-language model CLIP [12] with a separate LiDAR branch, which is trained with multi-modal contrastive learning [13], [15], [35]. However, the outlined approaches require aligned multi-modal sensor input and only focus on training a LiDAR encoder from scratch. Additionally, self-supervised representation learning requires a large amount of data, which is not readily available in the LiDAR domain, where large domain gaps exist between various sensors. We argue that leveraging pre-trained vision transformers directly is more efficient and suitable for small data problems.

Parameter-Efficient Fine-tuning: This research field aims to adapt strong foundation models to a specific task with minimal parameter updates. A common practice is to restrict weight updates to bias terms only [36]. Alternatively, visual prompt tuning (VPT) [36] inserts additional parameters in the form of learnable prompts into the transformer backbone. The family of LoRA adaptation [37] focuses on continuously attaching trainable rank decomposition matrices in parallel to a frozen transformer block. To enhance performance on dense prediction tasks, ViT-Adapter [38] introduces a spatial prior module as a separate convolutional stem that interacts with the main network branch through cross-attention.

For dense 3D point clouds, various adapters target the transformation of 3D pre-trained models (e.g., PointBERT [39]) for single-object classification and part segmentation. IDPT [40], PPT [41], and DAPT [21] enhance pre-trained models with learnable prompts. PointGST [20] motivates the usage of a spectral input representation to enhance the spatial correlation of 3D pre-trained tokens [20]. However, prior work shows that frozen vision or language foundation backbones paired with 3D-tailored adaptation mechanisms can surpass self-supervised 3D pre-training for single-object 3D segmentation [15], [42]–[44]. For example, Any2Point projects a point cloud into multiple 2D views and introduces an adapter tailored for local spatial aggregation and weighted feature ensembling [42]. On the other hand, PointFormer shows the benefit of applying a standard 2D adaptation mechanism [43]. However, existing adapter-based methods are limited to single-object, dense point cloud settings. Motivated by this line of work, we propose BALViT which is, to the best of our knowledge, the first 2D-3D adapter for sparse, outdoor point cloud processing. Our adapter enhances a frozen vision model with spatial priors retrieved from two complementary point cloud representations.

III. TECHNICAL APPROACH

Our proposed BALViT is tailored for adapting pre-trained vision transformer (ViT) backbones for LiDAR semantic segmentation. We argue that these architectures enable amodal feature encoding, which we enhance with our label-efficient 2D-3D adapter. Specifically, we first encode the point cloud in two separate branches, a range-view (RV) and a BEV encoder.

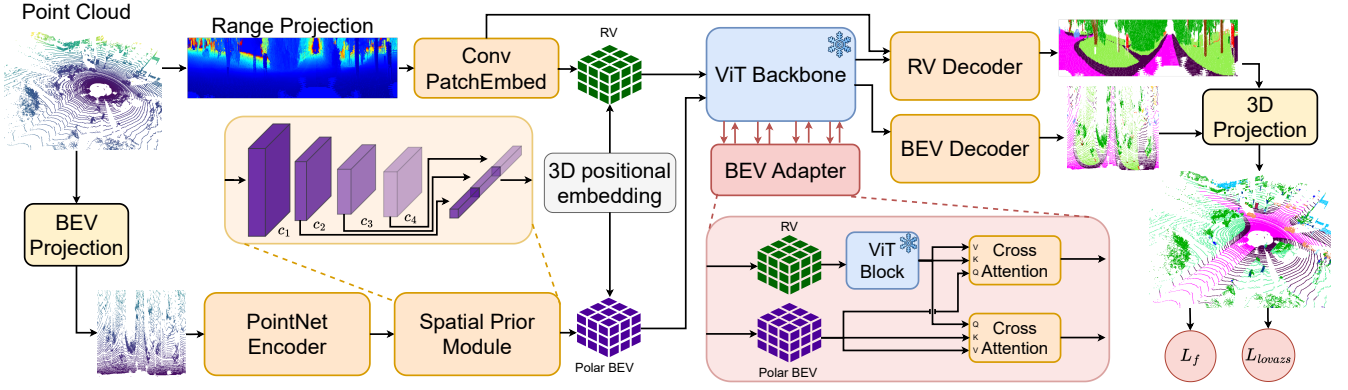


Fig. 2. Our network BALViT encodes a point cloud in orthogonal range-view (RV) and bird-eye-view (BEV) branches. Our spatial prior module converts the BEV branch into multi-scale features, which interact with the RV branch during its traversal of the frozen ViT backbone. Last, our two decoders independently obtain pointwise class labels from the respective feature maps.

Next, the RV features are processed by a frozen ViT backbone. During this backbone traversal, our novel 2D-3D adapter enables bidirectional feature enhancement between RV and BEV representations. Finally, we decode each feature branch with separate 3D decoders to combine the strengths of both views, effectively reducing misclassifications. Fig. 2 provides an overview of our architecture. In Sec. III-A and Sec. III-B, we outline the employed point cloud representations and encoding branches. Then, we introduce our proposed 2D-3D adapter in Sec. III-C, and finally we provide a description of the decoders in Sec. III-D.

A. Range-View Encoding

The input to our architecture is a LiDAR point cloud $P \in \mathbb{R}^{N \times 4}$ composed of N points, each with four values (x, y, z, i) . The variables (x, y, z) refer to the Cartesian coordinates and i represents the observed intensity of the returned LiDAR beam. To convert the LiDAR point cloud into a range projection of size $H \times W$, we first compute the pixel coordinates for each point $p_j \in P$ as follows:

$$\begin{bmatrix} h_j \\ w_j \end{bmatrix} = \begin{bmatrix} \frac{1}{2} (1 - \arctan(y_j, x_j) \frac{1}{\pi}) W \\ \left(1 - \left(\arcsin(z_j, \frac{1}{r_j}) - \frac{f_{\text{down}}}{f_v}\right)\right) H \end{bmatrix}, \quad (1)$$

where $r_j = \sqrt{x_j^2 + y_j^2 + z_j^2}$ corresponds to the range of the point p_j and $f_v = f_{\text{up}} - f_{\text{down}}$ being the vertical view of the LiDAR sensor [19]. We then construct the RV image I^{RV} according to Eq. (2) below:

$$I_{h_j, w_j}^{RV} = [r_j, z_j, i_j]. \quad (2)$$

When multiple points are mapped to the same pixel within I^{RV} , we select the one with the smallest range. We posit that range-views are best suited for direct processing with a pre-trained ViT backbone since this representation most closely resembles camera images. To encode images, a ViT backbone [45] commonly applies a single linear projection. To bridge the domain gap between camera images and I^{RV} , we replace this layer with our Conv PatchEmbed block that is composed of four residual blocks inspired by SalsaNext [46]. We later refer to features after this operation as RV_{stem} . We

employ average pooling with a kernel size of (PH_{RV}, PW_{RV}) and a final 1×1 convolution to convert RV_{stem} to have D_{RV} channels. Finally, we add a classification token and 2D positional embedding $E_{2D} \in \mathbb{R}^{(M+1) \times D_{RV}}$ to transfer the flattened M features into a suitable format for further encoding by the ViT backbone [19].

B. Polar Bird-Eye View Encoding

We complement the RV features with an orthogonal BEV branch. Specifically, we use a polar BEV representation I^{BEV} with grid cell dimension H_{BEV} , W_{BEV} , and Z_{BEV} . Therefore, we first convert the (x_j, y_j, z_j) coordinates of each point p_j into polar coordinates according to:

$$\begin{bmatrix} \rho_j \\ \phi_j \\ \theta_j \end{bmatrix} = \begin{bmatrix} \sqrt{x_j^2 + y_j^2} \\ -\arctan 2(y_j, -x_j) \\ \frac{(z_j - z_{\min})}{z_{\max} - z_{\min}} Z_{BEV} \end{bmatrix} \quad (3)$$

where z_{\min} and z_{\max} represent the minimum and maximum height, respectively. Then, we randomly select N_p points per BEV grid cell and leverage a PointNet-inspired encoder [24] consisting of 4 blocks of fully-connected layers, BatchNorm, and ReLU to compute an embedding of dimension D_{BEV} for each point. Next, we perform max pooling over the Z_{BEV} -dimension to obtain our BEV features of dimensionality $(D_{BEV}, H_{BEV}, W_{BEV})$. We create multi-scale BEV features with our spatial prior module to improve the model's capability to capture contextual information. This module consists of a ResNet-inspired stem and three convolutional blocks to transform the acquired BEV features into multi-scale representations $c1, c2, c3, c4$ with resolutions $(H_{BEV}/2, W_{BEV}/2), (H_{BEV}/4, W_{BEV}/2), (H_{BEV}/8, W_{BEV}/2)$ and $(H_{BEV}/8, W_{BEV}/2)$. Further, our spatial prior module transforms the channel dimension to D_{RV} in order to align with the RV features.

Subsequently, we add a 2D learnable positional embedding to the multi-scale features to preserve information about their respective scales when flattening them for further interactions in the 2D-3D adapter. We argue that these orthogonal LiDAR encoding mechanisms, RV-based and BEV-based,

are crucial for our method since they learn complementary point cloud representations whose combination transforms the ViT backbone into a strong LiDAR encoder.

C. 2D-3D Adapter Module

Before combining the two encoder branches, we add 3D positional embeddings $E_{3D} \in \mathbb{R}^{(M+1) \times D_{RV}}$ to both feature maps. Our sinusoidal positional embedding is computed separately in x , y , and z dimensions following the original transformer’s positional encoding [47]. Then, we concatenate the component-wise embeddings and upscale the resulting vector with two 1×1 convolutions to obtain a positional embedding of dimension D_{RV} . We leverage the transformations in Eq. (1) and Eq. (3) to extract the Cartesian coordinates of each feature in the two views, RV and BEV. We then use these geometric positions to infer their positional embeddings and add them to the respective feature maps independently. Our 3D positional embedding ensures that the interactions between the feature maps take into account the spatial geometries of the 3D scene. We emphasize the need for this positional embedding in Sec. IV-D.

The RV features are further encoded through subsequent blocks of the frozen ViT backbone. We perform feature integration of our two branches (RV and BEV) at different layers of the ViT backbone using our tailored interaction modules. Each interaction entails two parallel injector modules where one injector module (INJ) updates the features of one network branch (X) by performing sparse cross-attention with the other branch (Y) following Eq. (4), where γ_i is a learnable parameter. The second injector performs the same operation but with reversed branches.

$$X_i = X_i + \gamma_i \text{Attention}(\text{norm}(X_i), \text{norm}(Y_i)) \quad (4)$$

Our parallel stacked cross-attentions enhance the RV features from the frozen ViT backbone branch with domain-specific knowledge from the BEV branch (X=RV, Y=BEV), while at the same time, the BEV features are refined with novel context from the RV features (X=BEV, Y=RV). We note that it’s crucial that the interactions are performed in parallel to maximize the information flow between the two feature branches. Specifically, this operation ensures that information is continuously encoded and refined without one branch being more prominent. We ablate different configurations of the cross-attention layer in Sec. IV-D. We repeat these interactions after layers 5, 11, 17, and 23 of the ViT backbone. Since the backbone is frozen, only the weights of the interaction modules are updated, which results in our method being parameter-efficient. Consequently, we emphasize the suitability of our method for small datasets.

D. Decoder

We attach separate LiDAR decoders to the RV and BEV network branches to predict semantic segmentation on each view independently. For the RV branch, we use the decoder proposed by RangeViT [19], which is composed of a convolutional decoder, a PixelShuffle layer, and a 3D refiner. For the BEV branch, we propose a progressive decoder to

combine the multi-scale BEV feature maps. Our decoder fuses multi-scale features in a hierarchical manner: c_4 is first combined with c_3 , then upsampled and merged with c_2 , and finally upsampled again before integrating with c_1 . Last, we upsample the feature map to the original BEV input resolution using PixelShuffle [48], which helps maintain the integrity of point clouds. We then use three blocks of convolutions to recover the Z_{BEV} -dimension and predict a semantic class for every BEV cell grid. Finally, we employ a grid sampler to reproject our polar BEV predictions from polar ($S, W_{BEV}, H_{BEV}, Z_{BEV}$) to 3D coordinates (x, y, z) as detailed in Sec. III-B, where S is the number of classes.

We train our network using multi-class Focal [49] and Lovász-Softmax [50] losses separately for each decoder branch’s pointwise predictions. During inference, we merge pointwise RV and BEV predictions according to a predefined threshold t :

$$\text{Output} = \begin{cases} \hat{y}_{RV}, & \text{if } \hat{y}_{RV} > t \\ \hat{y}_{RV} & \text{if } \hat{y}_{RV} \leq t \text{ and } \hat{y}_{BEV} < t, \\ \hat{y}_{BEV}, & \text{if } \hat{y}_{RV} \leq t \text{ and } \hat{y}_{BEV} > t \end{cases} \quad (5)$$

where \hat{y}_{RV} and \hat{y}_{BEV} are the highest scores of the RV and BEV predictions, respectively. With the introduced merging mechanism, we can correct misclassifications in the RV feature branch, which results in a further boost in performance as presented in Sec. IV-D.

IV. EXPERIMENTAL EVALUATION

In this section, we quantitatively and qualitatively evaluate the performance of BALViT on LiDAR semantic segmentation and also provide a comprehensive ablation study to demonstrate the significance of our contribution. We first present an overview of the used datasets and then describe the experimental settings.

A. Datasets

We evaluated our proposed method on two autonomous driving datasets, SemantiKITTI and nuScenes.

SemantiKITTI [51]: This dataset is derived from the KITTI Odometry benchmark and consists of a total of 19,130 training and 4,071 validation scans. The dataset was collected with a single Velodyne HDL-64E LiDAR, which is mounted on a car driving around the city of Karlsruhe, Germany. The dataset provides point-wise labels for 19 semantic classes.

nuScenes [52]: This dataset consists of 28,130 training and 6,019 validation scans, which have been recorded in 1,000 scenes of 20 seconds each in Boston and Singapore. The LiDAR sensor that was used has 32 laser beams, and 16 semantic classes are annotated.

B. Experimental Setup

We use RV projections of size (64, 2048) with the patch size being defined as $PW_{rv} = 8$ and $PH_{rv} = 2$. We set the dimensionality of our RV features to $D_{rv} = 384$. Our polar BEV representation contains $480 \times 360 \times 32$ grid cells for the full point cloud, with each feature having $D_{bev} = 512$ dimensions. We define $z_{min}=-1$ and $z_{max}=3$. We use a

TABLE I
 LABEL-EFFICIENT TRAINING RESULTS ON 0.1%, 1%, 10% OF THE SEMANTICKITTI AND nuScenes DATASETS.

Method		SemanticKITTI mIoU (%)			nuScenes mIoU (%)		
		0.1%	1 %	10%	0.1%	1 %	10%
Fully-Supervised	Minkowski SR-Unet18 [53]	-	39.50	-	-	30.30	56.15
	FRNet [28]	30.09	40.78	61.55	28.03	48.98	69.99
	SphereFormer [23]	29.21	42.81	58.81	30.42	50.06	69.25
	RangeViT [19]	28.74	43.53	58.53	27.79	52.88	71.84
Vision Distillation	SLiDR [34]	-	44.60	-	-	38.30	59.84
	ST-SLiDR [54]	-	44.72	-	-	40.75	60.75
	SEAL [3]	-	46.63	-	-	45.84	62.97
	CLIP2Scene [13]	-	42.60	-	-	56.30	-
Parameter-Efficient Fine-Tuning	Frozen ViT backbone	29.97	45.91	58.10	28.72	54.70	63.28
	Bias tuning	30.86	45.63	58.14	28.15	56.05	65.08
	LoRA [37]	31.65	46.27	59.53	28.27	57.57	66.38
	VPT [36]	31.07	46.08	58.38	29.68	55.67	65.52
	Vit Adapter [38]	29.55	45.01	57.43	27.50	56.06	67.71
	BALViT (Ours)	32.85	51.80	61.91	31.86	59.27	70.13

The results are reported on the val set, and all metrics are in [%].

Cityscapes pre-trained ViT-S backbone for our model and show the effect of different pretrainings in Sec. IV-D.2. We train our networks and baselines for 100, 500, and 1000 epochs with dataset splits of 0.1%, 1%, and 10%, respectively. We use the SLiDR [54] protocol to create training subsets via uniform sampling, e.g. selecting every 100th frame for the 1% subset. We use a batch size of 4, a learning rate of 0.0004, and a cosine learning rate scheduler with 20 warm-up epochs. Further, we take random RV crops of size (64, 384) for SemanticKITTI and (64, 768) for nuScenes. Consequently, we equally subsample our BEV features, resulting in polar grid sizes of $480 \times 68 \times 32$ and $480 \times 135 \times 32$, respectively. We augment the point clouds with random horizontal flips with a probability of 0.5 and scale the point cloud in ranges of [0.95-1.05]. Further, we randomly resample rare class points. For nuScenes, we additionally randomly rotate in all three axes in the range of -5 and 5 degrees with a 50% probability. We set the inference threshold t to 0.9.

C. Quantitative Results

We compare BALViT with four fully supervised and four vision model distillation approaches. We select fully supervised methods with model size comparable to our method and which achieve top performance on the SemanticKITTI 100% setting. We use the respective author’s published code and apply the same augmentations outlined in Sec. IV-B. The self-supervised methods SLiDR [34], ST-SLiDR [54], SEAL [3] and CLIP2Scene [13] pretrain the Minkowski SR-Unet18 architecture [53] on the entire nuScenes dataset. For these methods, we report the achieved performance from their respective published work. We also compare with five parameter-efficient fine-tuning methods that we integrated in the RangeViT architecture [19]. For a fair comparison, we apply the same training configurations as used in our method.

All models are evaluated with the mean intersection-over-union (mIoU) metric. Results on SemanticKITTI and nuScenes are presented in Tab. I. Notably, BALViT outperforms all supervised and self-supervised baselines by at least 1.44pp on the 0.1% and 1% settings. This can be attributed

to the strong vision priors from the pretrained ViT, which our model effectively enhances via our novel 2D-3D adapter. However, the difference in performance decreases for the 10% settings, indicating that LiDAR-specific transformers possess strong encoding capabilities but require a sufficiently large quantity of labeled data. We further analyze the model performances when training with higher quantities of data in Sec. IV-D.4. In the last block of rows of Tab. I, we compare several parameter-efficient methods applied to the same base architecture as used in our method. First, we find that parameter-efficient fine-tuning is preferred to full-finetuning (RangeViT) in all the evaluated scenarios. We conclude that 2D pre-trained networks provide strong priors for 3D segmentation, which benefits from enhancement rather than retraining. Our method outperforms other parameter-efficient fine-tuning methods by at least 1.80pp on the 1% and 10% training settings. We find that our novel method of combining RV and BEV features within a frozen ViT model adds domain-specific knowledge in the feature encoding process, which outperforms standard parameter-efficient vision approaches. We discuss the effects of different components of our method in Sec. IV-D.1.

D. Ablation Study

In this section, we study the impact of various network components and dataset settings on the performance of our approach. We perform all ablation experiments on the 1% SemanticKITTI setting unless otherwise stated.

1) *Influence of Network Components:* We sequentially analyze the effect of our proposed network components in Tab. II. In the first row, we display the achieved performance when using the RangeViT architecture with a frozen ViT backbone. Next, we show that applying our 2D-3D adapter with unaligned single-scale features results in a performance improvement of 2.62pp, which we attribute to the enhancement of RV features through our BEV feature branch. Further, the performance is improved by an additional 0.53pp when RV and BEV features are aligned with our introduced 3D positional embedding strategy. We reason this observation

TABLE II
ABLATION STUDY ON VARIOUS COMPONENTS OF BALViT ON 1%
SEMANTICKITTI TRAINING SETTING.

2D-3D Adapter	3D PE	SPM	BEV decoder	1%
				45.91
✓				48.53
✓	✓			49.06
✓	✓	✓		49.70
✓	✓	✓	✓	51.80

3D PE: 3D positional embedding, SPM: Spatial Prior Module.

TABLE III
COMPARISON WITH DIFFERENT VISION BACKBONES ON 1%
SEMANTICKITTI TRAINING SETTING.

Backbone initialization	1 %
Supervised random init. †	44.58
Depth Anything [55]	45.11
Dino [56]	46.94
Dino v2 [11]	47.65
MoCov3 [57]	48.47
Supervised ImageNet [58]	48.68
Cityscapes [59]	51.80

†: vision backbone is updated during training.

with an improved cross-attention between geometric-aligned features. Next, we emphasize the importance of creating multi-scale BEV features and show that the observed performance is further improved by 0.63pp. Finally, we observe an improvement of 2.1pp when incorporating our BEV decoder into the network. We find that miss projections and semantic miss-classification can be reduced when guiding the prediction by two independent decoders.

2) *Influence of Pre-trained Vision Backbone:* We compare the performances when using different backbone pretrainings in Tab. III. In line with [19], we find that using a Cityscapes pretrained network results in the highest score. We posit that BALViT benefits from leveraging a vision backbone pre-trained on a closely related training domain (i.e., visual autonomous driving). Further, we record the lowest performance when leveraging a random initialized but trainable ViT backbone, which underscores the essential role of pretrained vision models when only a small amount of labels (1%) is available. We observe the second lowest performance on a Depth Anything pre-trained model, which we attribute to the difference in target task, depth estimation instead of semantic segmentation.

3) *Influence of Injector Modules:* As described in Sec. III-C, we perform our two injector operations (INJ) in parallel to enhance the information flow between the two feature branches. In this section, we study the order of operations in our 2D-3D adapter module. Specifically, we analyze the impact of applying one injector before a ViT block and the second INJ after the same block in Tab. IV. In the first row, we refine the BEV features before the block and the RV feature after, while in the second row we reverse the order. In the third row, we show that applying both injection operations in parallel results in the highest performance. These results

TABLE IV
ABLATION STUDY ON VARYING SEQUENCES OF INJECTOR (INJ) ON 1%
SEMANTICKITTI TRAINING SETTING.

Injector strategy	1 %
$\text{INJ}_{bev,rv} \rightarrow \text{ViTBlock} \rightarrow \text{INJ}_{rv,bev}$	46.17
$\text{INJ}_{rv,bev} \rightarrow \text{ViTBlock} \rightarrow \text{INJ}_{bev,rv}$	48.42
$\text{ViTBlock} \rightarrow \text{INJ}_{rv,bev} \parallel \text{INJ}_{bev,rv}$	51.80

TABLE V
PERFORMANCE ON 100% SEMANTICKITTI TRAINING DATA.

Method	100 %
SphereFormer	67.8 †
FRNet	68.7 †
RangeViT [19]	60.28
Frozen ViT	60.51
Bias tuning [36]	61.94
LoRA [37]	59.53
VPT [36]	61.46
Vit Adapter [38]	61.29
BALViT (Ours)	62.37

†: performance recorded in published work.

show that parallel injectors enhance the learning of different aspects simultaneously, which allows the network to capture more diverse features.

4) *Influence of Increased Training Data:* We emphasize that our method is designed for small data regimes, whereas tailored LiDAR architectures benefit from training on more data, as shown in Tab. V. Thus, we argue that when large quantities of data are available, LiDAR-specific models are preferred. Nevertheless, we show that our method also outperforms full fine-tuning of the RangeViT architecture when training on 100% of the dataset, confirming the impact of our 2D-3D adapter and independent decoder branches.

E. Qualitative Results

We further evaluate the impact of BALViT by qualitatively comparing its predictions with the second best-performing parameter-efficient method LoRA [37] in Fig. 3. Our qualitative analysis confirms the improved performance of BALViT. On both datasets, our method yields more coherent segmentation, resulting in stable prediction, less “patchified” regions, and fewer misclassifications. While LoRA misclassifies entire objects as marked blue in a), d), and g), BALViT effectively predicts the correct label for the complete instance due to our independent decoder branches, which counteract misclassifications of rare classes. Further, our method better captures finer semantic differences between terrain and vegetation as marked in red in c). However, we note that both LoRA and our method misclassify vegetation as trunk in c), which demonstrates that both methods are constrained by the diversity of input samples in this label-efficient setting.

We also observe that BALViT shows better performance on segmenting larger objects (e.g., truck, bus and other-vehicles) as shown in black in b), and f), which likely arises from an improved localization guidance. We find that our method improves semantic knowledge in label-efficient

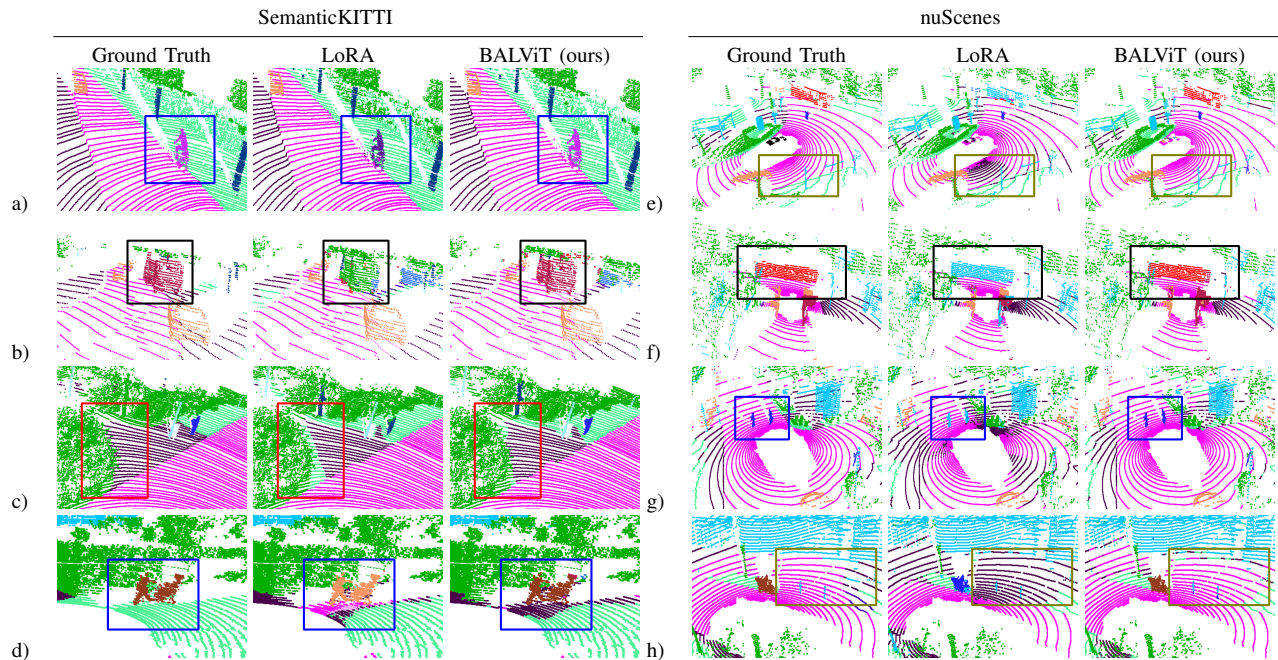


Fig. 3. Qualitative results of BALViT on LiDAR semantic segmentation on nuScenes and SemanticKITTI.

training regimes by aligning BEV and RV representations. Next, we observe much stronger localization and boundary-aware segments on the nuScenes dataset in e) and h) (green markings), where class boundaries for the semantic categories of sidewalk and road are more refined. We attribute this improvement to our multi-scale BEV features, which assist in capturing fine details.

V. CONCLUSION

We present BALViT, a novel method for LiDAR semantic segmentation tailored for small data regimes. Our approach encodes a RV projection with a frozen ViT backbone which we enhance with our 2D-3D adapter. Subsequently, we merge the predictions of our separate RV and BEV decoders for improved performance on rare classes. We observe that our approach outperforms existing state-of-the-art supervised and self-supervised baselines on label-efficient training settings of 0.1% and 1% on the SemanticKITTI and nuScenes datasets. The proposed method is one of the early works to show that 2D vision models provide valuable priors for LiDAR semantic scene segmentation. Consequently, we motivate future work to directly integrate pre-trained vision architectures in point cloud segmentation models to leverage future advancements in foundation model research.

REFERENCES

- [1] R. Mohan, D. Cattaneo, F. Drews, and A. Valada, "Progressive multi-modal fusion for robust 3d object detection," in *Annual Conf. on Robot Learning*, 2024.
- [2] C. Lang, A. Braun, L. Schillingmann, and A. Valada, "A point-based approach to efficient lidar multi-task perception," in *Proc. IEEE Int. Conf. on Intel. Rob. and Syst.*, 2024, pp. 13 261–13 268.
- [3] Y. Liu, L. Kong, J. CEN, R. Chen, W. Zhang, L. Pan, K. Chen, and Z. Liu, "Segment any point cloud sequences by distilling vision foundation models," in *Adv. Neural Inform. Process. Syst.*, 2023.
- [4] L. Nunes, L. Wiesmann, R. Marcuzzi, X. Chen, J. Behley, and C. Stachniss, "Temporal consistent 3d lidar representation learning for semantic perception in autonomous driving," in *Proc. IEEE Conf. Comput. Vis. Pattern Recog.*, 2023, pp. 5217–5228.
- [5] L. Nunes, R. Marcuzzi, X. Chen, J. Behley, and C. Stachniss, "Seg-contrast: 3d point cloud feature representation learning through self-supervised segment discrimination," *IEEE Robotics and Automation Letters*, vol. 7, no. 2, pp. 2116–2123, 2022.
- [6] N. Gosala, K. Petek, P. L. Drews-Jr, W. Burgard, and A. Valada, "Skyeye: Self-supervised bird's-eye-view semantic mapping using monocular frontal view images," in *Proc. IEEE Conf. Comput. Vis. Pattern Recog.*, 2023, pp. 14 901–14 910.
- [7] C. Lang, A. Braun, L. Schillingmann, K. Haug, and A. Valada, "Self-supervised representation learning from temporal ordering of automated driving sequences," *IEEE Robotics and Automation Letters*, vol. 9, no. 3, pp. 2582–2589, 2024.
- [8] J. Hindel, N. Gosala, K. Bregler, and A. Valada, "Inod: Injected noise discriminator for self-supervised representation learning in agricultural fields," *IEEE Robotics and Automation Letters (RA-L)*, 2023.
- [9] B. Bešić, N. Gosala, D. Cattaneo, and A. Valada, "Unsupervised domain adaptation for lidar panoptic segmentation," *IEEE Robotics and Automation Letters*, vol. 7, no. 2, pp. 3404–3411, 2022.
- [10] A. Xiao, X. Zhang, L. Shao, and S. Lu, "A survey of label-efficient deep learning for 3d point clouds," in *IEEE Transactions on Pattern Analysis & Machine Intelligence*, vol. 46, no. 12, 2024, pp. 9139–9160.
- [11] M. Oquab, T. Darcet, T. Moutakanni, H. V. Vo, M. Szafraniec, V. Khalidov, P. Fernandez, D. HAZIZA, F. Massa, A. El-Nouby, M. Assran, N. Ballas, W. Galuba, R. Howes, P.-Y. Huang, S.-W. Li, I. Misra, M. Rabbat, V. Sharma, G. Synnaeve, H. Xu, H. Jegou, J. Mairal, P. Labatut, A. Joulin, and P. Bojanowski, "DINOv2: Learning robust visual features without supervision," *Transactions on Machine Learning Research*, 2024.
- [12] A. Radford, J. W. Kim, C. Hallacy, A. Ramesh, G. Goh, S. Agarwal, G. Sastry, A. Askell, P. Mishkin, J. Clark, G. Krueger, and I. Sutskever, "Learning transferable visual models from natural language supervision," in *International Conference on Machine Learning*, 2021.
- [13] R. Chen, Y. Liu, L. Kong, X. Zhu, Y. Ma, Y. Li, Y. Hou, Y. Qiao, and W. Wang, "Clip2scene: Towards label-efficient 3d scene understanding by clip," in *Proc. IEEE Conf. Comput. Vis. Pattern Recog.*, 2023.
- [14] J. Zhou, J. Wang, B. Ma, Y.-S. Liu, T. Huang, and X. Wang, "Uni3d: Exploring unified 3d representation at scale," in *Int. Conf. Learn. Represent.*, 2024.
- [15] D. Hegde, J. M. J. Valanarasu, and V. M. Patel, "Clip goes 3d:

- Leveraging prompt tuning for language grounded 3d recognition,” *arXiv preprint arXiv:2303.11313*, 2023.
- [16] Y. Zeng, C. Jiang, J. Mao, J. Han, C. Ye, Q. Huang, D.-Y. Yeung, Z. Yang, X. Liang, and H. Xu, “Clip2: Contrastive language-image-point pretraining from real-world point cloud data,” in *Proc. IEEE Conf. Comput. Vis. Pattern Recog.*, 2023, pp. 15 244–15 253.
- [17] X. Zhu, R. Zhang, B. He, Z. Guo, Z. Zeng, Z. Qin, S. Zhang, and P. Gao, “Pointclip v2: Prompting clip and gpt for powerful 3d open-world learning,” in *Proc. Int. Conf. Comput. Vis.*, 2023, pp. 2639–2650.
- [18] X. Xu, L. Kong, H. Shuai, W. Zhang, L. Pan, K. Chen, Z. Liu, and Q. Liu, “4d contrastive superflows are dense 3d representation learners,” in *Proc. Springer Eur. Conf. Comput. Vis.*, 2024, pp. 58–80.
- [19] A. Ando, S. Gidaris, A. Bursuc, G. Puy, A. Boulch, and R. Marlet, “Rangevit: Towards vision transformers for 3d semantic segmentation in autonomous driving,” *Proc. IEEE Conf. Comput. Vis. Pattern Recog.*, pp. 5240–5250, 2023.
- [20] D. Liang, T. Feng, X. Zhou, Y. Zhang, Z. Zou, and X. Bai, “Parameter-efficient fine-tuning in spectral domain for point cloud learning,” *arXiv preprint arXiv:2410.08114*, 2024.
- [21] X. Zhou, D. Liang, W. Xu, X. Zhu, Y. Xu, Z. Zou, and X. Bai, “Dynamic adapter meets prompt tuning: Parameter-efficient transfer learning for point cloud analysis,” in *Proc. IEEE Conf. Comput. Vis. Pattern Recog.*, 2024, pp. 14 707–14 717.
- [22] X. Zhu, H. Zhou, T. Wang, F. Hong, Y. Ma, W. Li, H. Li, and D. Lin, “Cylindrical and asymmetrical 3d convolution networks for lidar segmentation,” in *Proc. IEEE Conf. Comput. Vis. Pattern Recog.*, 2021, pp. 9939–9948.
- [23] X. Lai, Y. Chen, F. Lu, J. Liu, and J. Jia, “Spherical transformer for lidar-based 3d recognition,” in *Proc. IEEE Conf. Comput. Vis. Pattern Recog.*, 2023.
- [24] C. Qi, H. Su, K. Mo, and L. J. Guibas, “Pointnet: Deep learning on point sets for 3d classification and segmentation,” *Proc. IEEE Conf. Comput. Vis. Pattern Recog.*, pp. 77–85, 2016.
- [25] X. Wu, L. Jiang, P.-S. Wang, Z. Liu, X. Liu, Y. Qiao, W. Ouyang, T. He, and H. Zhao, “Point transformer v3: Simpler faster stronger,” in *Proc. IEEE Conf. Comput. Vis. Pattern Recog.*, 2024, pp. 4840–4851.
- [26] X. Wu, Y. Lao, L. Jiang, X. Liu, and H. Zhao, “Point transformer v2: Grouped vector lattention and partition-based pooling,” in *Adv. Neural Inform. Process. Syst.*, 2022.
- [27] Y. Zhang, Z. Zhou, P. David, X. Yue, Z. Xi, B. Gong, and H. Foroosh, “Polarnet: An improved grid representation for online lidar point clouds semantic segmentation,” in *Proc. IEEE Conf. Comput. Vis. Pattern Recog.*, 2020, pp. 9601–9610.
- [28] X. Xu, L. Kong, H. Shuai, and Q. Liu, “Frnet: Frustum-range networks for scalable lidar segmentation,” *arXiv preprint arXiv:2312.04484*, 2023.
- [29] L. Kong, Y. Liu, R. Chen, Y. Ma, X. Zhu, Y. Li, Y. Hou, Y. Qiao, and Z. Liu, “Rethinking range view representation for lidar segmentation,” in *Proc. IEEE Conf. Comput. Vis. Pattern Recog.*, 2023, pp. 228–240.
- [30] C. Sautier, G. Puy, A. Boulch, R. Marlet, and V. Lepetit, “BEVContrast: Self-supervision in bev space for automotive lidar point clouds,” in *International Conference on 3D Vision (3DV)*, 2024.
- [31] Z. Zhang, M. Bai, and L. E. Li, “Implicit surface contrastive clustering for lidar point clouds,” in *Proc. IEEE Conf. Comput. Vis. Pattern Recog.*, 2023, pp. 21 716–21 725.
- [32] A. Boulch, C. Sautier, B. Michele, G. Puy, and R. Marlet, “Also: Automotive lidar self-supervision by occupancy estimation,” in *Proc. IEEE Conf. Comput. Vis. Pattern Recog.*, 2023, pp. 13 455–13 465.
- [33] G. Puy, S. Gidaris, A. Boulch, O. Siméoni, C. Sautier, P. Pérez, A. Bursuc, and R. Marlet, “Three pillars improving vision foundation model distillation for lidar,” in *Proc. IEEE Conf. Comput. Vis. Pattern Recog.*, 2024, pp. 21 519–21 529.
- [34] C. Sautier, G. Puy, S. Gidaris, A. Boulch, A. Bursuc, and R. Marlet, “Image-to-lidar self-supervised distillation for autonomous driving data,” in *Proc. IEEE Conf. Comput. Vis. Pattern Recog.*, 2022.
- [35] L. Xue, M. Gao, C. Xing, R. Martín-Martín, J. Wu, C. Xiong, R. Xu, J. C. Niebles, and S. Savarese, “Ulip: Learning a unified representation of language, images, and point clouds for 3d understanding,” in *Proc. IEEE Conf. Comput. Vis. Pattern Recog.*, 2023, pp. 1179–1189.
- [36] M. Jia, L. Tang, B.-C. Chen, C. Cardie, S. Belongie, B. Hariharan, and S.-N. Lim, “Visual prompt tuning,” in *European Conference on Computer Vision*, 2022, pp. 709–727.
- [37] E. J. Hu, Y. Shen, P. Wallis, Z. Allen-Zhu, Y. Li, S. Wang, L. Wang, and W. Chen, “LoRA: Low-rank adaptation of large language models,” in *Int. Conf. Learn. Represent.*, 2022.
- [38] Z. Chen, Y. Duan, W. Wang, J. He, T. Lu, J. Dai, and Y. Qiao, “Vision transformer adapter for dense predictions,” in *Int. Conf. Learn. Represent.*, 2023.
- [39] X. Yu, L. Tang, Y. Rao, T. Huang, J. Zhou, and J. Lu, “Point-bert: Pre-training 3d point cloud transformers with masked point modeling,” in *Proc. IEEE Conf. Comput. Vis. Pattern Recog.*, 2022.
- [40] Y. Zha, J. Wang, T. Dai, B. Chen, Z. Wang, and S.-T. Xia, “Instance-aware dynamic prompt tuning for pre-trained point cloud models,” in *Proc. Int. Conf. Comput. Vis.*, 2023, pp. 14 115–14 124.
- [41] B. Fei, L. Liu, W. Yang, Z. Li, W.-M. Chen, and L. Ma, “Parameter efficient point cloud prompt tuning for unified point cloud understanding,” *IEEE Transactions on Intelligent Vehicles*, pp. 1–16, 2024.
- [42] Y. Tang, R. Zhang, J. Liu, Z. Guo, B. Zhao, Z. Wang, P. Gao, H. Li, D. Wang, and X. Li, “Any2point: Empowering any-modality large models for efficient 3d understanding,” in *Proc. Springer Eur. Conf. Comput. Vis.*, 2022, pp. 456–473.
- [43] M. Li, D. Li, G. Yang, Y.-m. Cheung, and H. Huang, “Adapt pointformer: 3d point cloud analysis via adapting 2d visual transformers,” *arXiv preprint arXiv:2407.13200*, 2024.
- [44] X. Huang, Z. Huang, S. Li, W. Qu, T. He, Y. Hou, Y. Zuo, and W. Ouyang, “Frozen clip transformer is an efficient point cloud encoder,” in *Proceedings of the AAAI Conference on Artificial Intelligence*, vol. 38, no. 3, 2024, pp. 2382–2390.
- [45] A. Dosovitskiy, L. Beyer, A. Kolesnikov, D. Weissenborn, X. Zhai, T. Unterthiner, M. Dehghani, M. Minderer, G. Heigold, S. Gelly, J. Uszkoreit, and N. Houlsby, “An image is worth 16x16 words: Transformers for image recognition at scale,” *Int. Conf. Learn. Represent.*, 2021.
- [46] T. Cortinhal, G. Tzelepis, and E. Erdal Aksoy, “Salsanext: Fast, uncertainty-aware semantic segmentation of lidar point clouds,” in *Int. Symp. on Advances in Visual Computing*, 2020, pp. 207–222.
- [47] A. Vaswani, N. Shazeer, N. Parmar, J. Uszkoreit, L. Jones, A. N. Gomez, Ł. Kaiser, and I. Polosukhin, “Attention is all you need,” *Adv. Neural Inform. Process. Syst.*, vol. 30, 2017.
- [48] W. Shi, J. Caballero, F. Huszár, J. Totz, A. P. Aitken, R. Bishop, D. Rueckert, and Z. Wang, “Real-time single image and video super-resolution using an efficient sub-pixel convolutional neural network,” in *Proc. IEEE Conf. Comput. Vis. Pattern Recog.*, 2016, pp. 1874–1883.
- [49] T.-Y. Lin, P. Goyal, R. B. Girshick, K. He, and P. Dollár, “Focal loss for dense object detection,” *Proc. Int. Conf. Comput. Vis.*, 2017.
- [50] M. Berman, A. Rannen Triki, and M. B. Blaschko, “The lovasz-softmax loss: A tractable surrogate for the optimization of the intersection-over-union measure in neural networks,” in *Proc. IEEE Conf. Comput. Vis. Pattern Recog.*, 2018, pp. 4413–4421.
- [51] J. Behley, M. Garbade, A. Milioto, J. Quenzel, S. Behnke, C. Stachniss, and J. Gall, “SemanticKITTI: A Dataset for Semantic Scene Understanding of LiDAR Sequences,” in *Proc. Int. Conf. Comput. Vis.*, 2019.
- [52] H. Caesar, V. Bankiti, A. H. Lang, S. Vora, V. E. Liong, Q. Xu, A. Krishnan, Y. Pan, G. Baldan, and O. Beijbom, “nusenes: A multimodal dataset for autonomous driving,” *Proc. IEEE Conf. Comput. Vis. Pattern Recog.*, pp. 11 618–11 628, 2019.
- [53] C. B. Choy, J. Gwak, and S. Savarese, “4d spatio-temporal convnets: Minkowski convolutional neural networks,” *Proc. IEEE Conf. Comput. Vis. Pattern Recog.*, pp. 3070–3079, 2019.
- [54] A. Mahmoud, J. S. K. Hu, T. Kuai, A. Harakeh, L. Paull, and S. L. Waslander, “Self-supervised image-to-point distillation via semantically tolerant contrastive loss,” *Proc. IEEE Conf. Comput. Vis. Pattern Recog.*, pp. 7102–7110, 2023.
- [55] L. Yang, B. Kang, Z. Huang, X. Xu, J. Feng, and H. Zhao, “Depth anything: Unleashing the power of large-scale unlabeled data,” in *Proc. IEEE Conf. Comput. Vis. Pattern Recog.*, 2024.
- [56] M. Caron, H. Touvron, I. Misra, H. Jégou, J. Mairal, P. Bojanowski, and A. Joulin, “Emerging properties in self-supervised vision transformers,” in *Proc. Int. Conf. Comput. Vis.*, 2021.
- [57] X. Chen*, S. Xie*, and K. He, “An empirical study of training self-supervised vision transformers,” *arXiv preprint arXiv:2104.02057*, 2021.
- [58] J. Deng, W. Dong, R. Socher, L.-J. Li, K. Li, and L. Fei-Fei, “Imagenet: A large-scale hierarchical image database,” in *Proc. IEEE Conf. Comput. Vis. Pattern Recog.*, 2009, pp. 248–255.
- [59] M. Cordts, M. Omran, S. Ramos, T. Rehfeld, M. Enzweiler, R. Benenson, U. Franke, S. Roth, and B. Schiele, “The cityscapes dataset for semantic urban scene understanding,” in *Proc. IEEE Conf. Comput. Vis. Pattern Recog.*, 2016.